Available online at www.sciencedirect.com
SCIENCE DIRECT
Biochemical Pharmacology 69 (2005) 1723–1732
Biochemical Pharmacology
www.elsevier.com/locate/biochempharm

Real-time measurement in living cells of insulin-like growth factor activity using bioluminescence resonance energy transfer

Lisbeth S. Laursen, Claus Oxvig *

Department of Molecular Biology, Science Park, University of Aarhus, Gustav Wieds Vej 10C, DK-8000 Aarhus C, Denmark

Received 16 March 2005; accepted 11 April 2005

Abstract

Insulin-like growth factor (IGF)-I and -II function in normal physiology to control growth, development, and differentiation, but are also important in pathophysiological conditions, particularly in cancer. The biological effects of the IGFs are mediated by the IGF-I receptor (IGFR), a covalent homodimer composed of two alpha and two beta chains, similar in structure to the insulin receptor (IR). To allow measurement of the stimulation of IGFR in living cells, we developed an assay based on bioluminescence resonance energy transfer (BRET) between a donor molecule, Renilla luciferase, and an acceptor fluorophore, enhanced yellow fluorescent protein (EYFP). Initial attempts based on fusion of the luciferase to IGFR, and EYFP to IGFR, or to downstream signaling molecules, insulin receptor substrate-1 (IRS1) or protein tyrosine phosphatases-1B (PTP-1B), failed. However, similar experiments with IR, carried our in parallel, proved successful. We therefore, constructed assays based on chimeric IGFR/IR proteins, in which the ligand binding site was derived from IGFR. With the most efficient assay, in which the luciferase is fused to a chimeric receptor with the entire intracellular portion derived from IR, and EYFP fused to PTP-1B, IGF activity was measured specifically with sensitivity similar to the corresponding assay for insulin, based on IR. The established system allows efficient evaluation of candidate ligand- or receptor-directed molecules for the modulation of IGF activities. Furthermore, we demonstrate that a set of inhibitory IGF binding proteins (IGFBPs) or activating IGFBP-specific proteinases, unique to the IGF system, may serve as potential targets. In addition to screening, real-time measurement of IGFR stimulation may be important in efforts to understand the kinetics of receptor stimulation, in particular differences between IGFR and IR.

Keywords: Insulin-like growth factor; Insulin; Receptor; Bioluminescence resonance energy transfer; Insulin-like growth factor binding proteins

1. Introduction

The insulin-like growth factors (IGF-I and -II) are ubiquitously expressed single-chain polypepides of 70 and 67 residues, respectively, homologous to the hormone insulin [1]. Unlike insulin, which plays a pivotal role in metabolic regulation, the IGFs function in normal physiology to control growth, development, and differentiation of cells [2].

However, IGF signaling is also involved in pathophysiological conditions. In particular, considerable evidence has recently accumulated to demonstrate the involvement of IGF signaling in development and progression of many different types of cancer. Individuals with elevated circulating levels of IGF have an increased risk of developing certain cancers, and IGFs are synthesized by tumor cells to possibly function in an autocrine manner [3–6]. It is therefore desirable to control the biological activities of the IGFs, either directly by the interference with receptor ligation, or by interference with downstream signaling, and such strategies for the prevention and treatment of cancer are being developed [7–10].

The biological effects of IGF-I and -II are mediated by the IGF-I receptor (IGFR), which belongs to the receptor tyrosine kinase (RTK) superfamily (Fig. 1A). During its biosynthesis, a single polypeptide is cleaved into an N-terminal α-subunit and a C-terminal β-subunit, which forms the final α2β2 structure with all four polypeptide chains held together by disulfide bonds. The two α-subunits form a single ligand binding site, and the transmembrane β-subunit harbors the intracellular tyrosine kinase domain which becomes autophosphorylated upon ligand binding [7]. The insulin receptor (IR) is similar in structure and shows 58% overall sequence identity with IGFR. There are two isoforms of IR, which differ by the absence (IR-A) or the presence (IR-B) of a 12-residue stretch in the C-ternimal end of the α-subunit, corresponding to exon 11 [11].

* Corresponding author. Tel.: +45 8942 5060; fax: +45 8942 5068.
E-mail address: co@mb.au.dk (C. Oxvig).

0006-2952/$ – see front matter © 2005 Elsevier Inc. All rights reserved.
doi:10.1016/j.bcp.2005.04.005

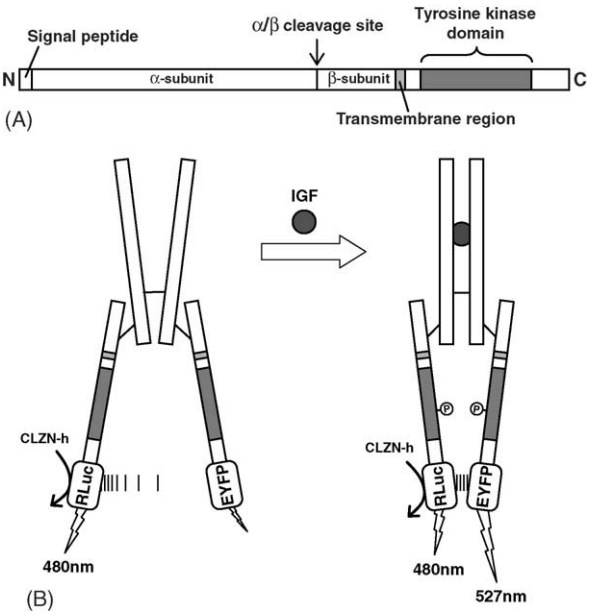

Fig. 1. The BRET methodology applied to IGFR. (A) Schematic representation of the unprocessed 1367-residue IGFR precursor. The N-terminus, the C-terminus, the signal peptide, the position of cleavage during receptor maturation, the membrane spanning region, and the kinase domain are indicated. The figure is drawn to scale. (B) When cells are co-transfected with cDNA encoding IGFR fused to the *Renilla* luciferase (RLuc) and enhanced yellow fluorescent protein (EYFP), respectively, half of the recombinant receptors will be mixed, as depicted. Three disulfide bonds are indicated as lines between the bars, and one predicted site of autophosphorylation is marked with a P. First, upon the addition of the RLuc substrate coelenterazine h (CLZN-h) to transfected cells, light at 480 nm is emitted (left). Second, upon receptor stimulation with IGF, conformational changes in the receptor are believed to occur (right). These changes are hypothesized to bring the RLuc and EYFP domains in closer proximity to each other, causing the transfer of excited-state energy from RLuc (the donor) to EYFP (the acceptor), and in turn an increase in emission of light at 527 nm from EYFP. Based on measurement of the emitted light at the two different wavelengths, the BRET ratio, proportional to the degree of receptor stimulation, is calculated.

The tyrosine kinase domains of IGFR and IR have several known, common substrates, including insulin receptor substrates-1 (IRS1), that mediate further progression of the signaling cascades [12]. There are also known differences in the signaling pathways, but details of how differential effects are mediated by the two receptors are still not clear [2,13]. It is generally believed that the activities of RTK receptors are negatively regulated by protein tyrosine phosphatases (PTPs). One such phosphatase, PTP-1B, has been shown to interact directly with both IGFR [14] and IR [15].

Unlike insulin, the IGFs are regulated by a set of six binding proteins (IGFBP-1 to IGFBP-6) which bind the IGFs with higher affinities than IGFR and thus, antagonize IGF activity [3]. The IGFBPs, in turn, are also subject to regulation, including proteolytic cleavage, which causes release of bound IGF [3]. Hence, control of IGF activity, whether physiologic or therapeutic, can possibly also be exerted by the interference with the release of IGF inactivated by IGFBPs.

We have developed an assay based on bioluminescence resonance energy transfer (BRET) that allows measurement of IGF activity in living cells. The established system allows efficient screening for molecules which modulate IGF activities. In addition, it may facilitate the biochemical study of IGF release from IGFBP–IGF complexes in proximity to the cell surface.

2. Materials and methods

2.1. Plasmid constructs

The following plasmids were constructed (Table 1).

2.1.1. pIGFR

The cDNA encoding human IGFR (nt 46-4149, accession number NM_000875; contained in pMJ-475, provided by C. Kristensen, Novo Nordic), was excised with *Bam*HI and cloned into the *Bam*HI site of pcDNA3.1(+) (Invitrogen) to generate pIGFR.

2.1.2. pIGFR–RLuc

For removal of the stop codon of the IGFR cDNA, and for fusion of its IGFR C-terminus to RLuc (i.e. in-frame fusion), a PCR fragment was generated using the primers 5′-GTGAGAGGATTGAGTTTCTC-3′ (nt. 3171-3189 of IGFR) and 5′-ACTGGGATCCGCAGGTCGAAGACTGGGGCAGC-3′ (nt 4146-4125, added *Bam*HI site is underlined), and pIGFR as the template. The *Hin*dIII–*Bam*HI fragment of the PCR product was ligated with the *Bam*HI–*Hin*dIII fragment of pIGFR into the *Bam*HI site of pRluc-N2 (BioSignal Packard), to generate pIGFR–RLuc.

2.1.3. pIGFR–EYFP

For in-frame fusion of the IGFR C-terminus to EYFP, a PCR fragment was generated using the primers 5′-GTGAGAGGATTGAGTTTCTC-3′ (nt. 3171-3189 of IGFR) and 5′-ACTGGGATCC**CG**GCAGGTCGAAGACTGGGGCAGC-3′ (nt 4146-4125, added *Bam*HI site is underlined, and nucleotides added for in-frame coding are shown in bold), and pIGFR as the template. The *Hin*dIII–*Bam*HI fragment of the PCR product was ligated with the *Bam*HI–*Hin*dIII fragment of pIGFR into the *Bam*HI site of pEYFP-N1 (BD Biosciences, Clontech), to generate pIGFR-EYFP.

2.1.4. pIRS1–EYFP

mRNA was isolated from human liver, and two PCR fragments covering the entire cDNA sequence of human IRS1 (nt 1021-4749, accession number NM_005544) were generated using oligo-dT-primed cDNA as the templates. The first PCR fragment was generated using the primers 5′-GTACAAGCTTATGGCGAGCCCTCCGGAGAGC-3′ (nt 1021-1041, added *Hin*dIII site underlined) and 5′-GCCCCTTGCCACCCATGCAGAT-3′ (nt 2437-2416). The second fragment was generated using the primers 5′-

Table 1
IGFR and IR expression constructs prepared for BRET analysis

Expression plasmid	Description[a]	Linker sequence[b]
pIGFR	Plasmid encodes human IGFR (res. 1-1367). Vector: pcDNA3.1(+)	None
pIGFR–RLuc	Plasmid encodes human IGFR (res. 1-1367) C-terminally fused to RLuc. Vector: pRluc-N2	GSPPARAT
pIGFR–EYFP	Plasmid encodes human IGFR (res. 1-1367) C-terminally fused to EYFP. Vector: pEYFP-N1	RDPPVAT
pIRS1–EYFP	Plasmid encodes human IRS1 (res. 1-1242) C-terminally fused to EYFP. Vector: pEYFP-N1	RDPPVAT
ptr-IRS1–EYFP	Plasmid encodes a truncated IRS1 variant (res. 1-262) C-terminally fused to EYFP. Vector: pEYFP-N1	RDPPVAT
pEYFP-PTP-1B	Plasmid encodes human PTP-1B (res. 1-435) N-terminally fused to EYFP. Vector: pcDNA3.1(+)	KLGTELGS
pEYFP-PTP-1B(D181A)	Plasmid is a mutated variant of pEYFP-PTP-1B, in which Asp-181 is mutated to Ala. Vector: pcDNA3.1(+)	KLGTELGS
pIR-B-RLuc	Plasmid encodes human IR-B (res. 1-1382) C-terminally fused to RLuc. Vector: pRluc-N3	GSPPARAT
pIR-B-EYFP	Plasmid encodes human IR-B (res. 1-1382) C-terminally fused to EYFP. Vector: pEYFP-N1	RDPPVAT
pIR-A-RLuc	Plasmid encodes human IR-A (res. 1-1382, excl. 744-755 corresponding to exon 11) C-terminally fused to RLuc. Vector: pRluc-N3	GSPPARAT
pIR-A-EYFP	Plasmid encodes human IR-A (res. 1-1382, excl. 744-755 corresponding to exon 11) C-terminally fused to EYFP. Vector: pEYFP-N1	RDPPVAT
pCH1	Plasmid encodes a chimeric receptor, IGFR(1-740)-IR-B(763-1382), C-terminally fused to RLuc. Vector: pRluc-N2	GSPPARAT
pCH2	Plasmid encodes a chimeric receptor, IGFR(1-936)-IR-B(957-1382), C-terminally fused to RLuc. Vector: pRluc-N2	GSPPARAT
pCH3	Plasmid encodes a chimeric receptor, IGFR(1-1274)-IR-B(1299-1382), C-terminally fused to RLuc. Vector: pRluc-N2	GSPPARAT
pCH1-EYFP	Plasmid encodes a chimeric receptor, IGFR(1-740)-IR-B(763-1382), C-terminally fused to EYFP. Vector: pEYFP-N1	RDPPVAT
pCH2-EYFP	Plasmid encodes a chimeric receptor, IGFR(1-936)-IR-B(957-1382), C-terminally fused to EYFP. Vector: pEYFP-N1	RDPPVAT
pCH3-EYFP	Plasmid encodes a chimeric receptor, IGFR(1-1274)-IR-B(1299-1382), C-terminally fused to EYFP. Vector: pEYFP-N1	RDPPVAT

[a] Numbering of amino acid sequences is according to the database accession numbers P08069 (IGFR), P06213 (IR-A and -B), NM_005544 (IRS1), and NM_002827 (PTP-1B).
[b] Amino acid sequences of linkers are given by one-letter code.

CGGATTCCCTGGGCCACACCC-3′ (nt 2360–2380) and 5′-GTACGGATCC**CG**CTGACGGTCCTCTGGTCTGCT-TC-3′ (nt 4746-4725, added *Bam*HI site underlined, and nucleotides added for in-frame coding are shown in bold). The *Hin*dIII–*Sac*II fragment of the first PCR and the appr. 2350 nt *Sac*II–*Bam*HI fragment of the second PCR were ligated together into the *Hin*dIII/*Bam*HI sites of pEYFP-N1, to generate pIRS1–EYFP, encoding wild-type IRS1 (1242 residues) fused to EYFP.

2.1.5. ptr-IRS1–EYFP

A PCR product was generated using the primers 5′-GTACAAGCTTATGGCGAGCCCTCCGGAGAG-3′ (nt 1021-1041, *Hin*dIII site underlined) and 5′-GTCAG-GATCC**CG**CTGGCTCTTGCTGCGAGGGCGGA-3′ (nt 1833-1811, *Bam*HI site underlined, and nucleotides added for in-frame coding are shown in bold) and pIRS1–EYFP as the template. The *Hin*dIII–*Bam*HI fragment of this product was cloned into the *Hin*dIII/*Bam*HI sites of pEYFP-N1, to generate ptr-IRS1–EYFP encoding residues 1-262 of IRS1 fused to EYFP.

2.1.6. pEYFP-PTP-1B

A PCR fragment encoding EYFP was generated using the primers 5′-GCACGCTAGCATGGTGAGCAAGGGC-GAGGAGC-3′ (nt 679-700 of pEYFP-N1, added *Nhe*I site underlined) and 5′-GCACAAGCTTTGATCTAGAGTC-GCGGCCGCTTTAC-3′ (nt 1396-1372 of pEYFP-N1, added *Hin*dIII site underlined) and pEYFP-N1 as the template. The fragment was cloned into the the *Nhe*I/*Hin*dIII sites of pcDNA3.1(+), to generate pcDNA3.1-EYFP. mRNA was isolated from human placenta, and a PCR fragments covering the entire cDNA sequence of human PTP-1B (nt 175-1482 of accession number NM_002827) was generated using oligo-dT-primed cDNA as the template, and the primers 5′-CTGAGGATCCATG-GAGATGGAAAAGGAGTTCGAGC-3′ (175-199, added *Bam*HI site underlined) and 5′-GCTAGAATTCCT-ATGTGTTGCTGTTGAACAGGAACC-3′ (1479-1456, added *Eco*RI site underlined). The PCR product was digested with *Bam*HI/*Eco*RI and cloned into pcDNA3.1-EYFP, to generate pEYFP-PTP-1B, in which the linker is encoded by the sequence between the *Hin*dIII

and the *Bam*HI sites of the pcDNA3.1(+) multiple cloning site.

2.1.7. pEYFP-PTP-1B(D181A)

A mutation (D181A) was introduced into PTP-1B of pEYFP-PTP-1B using overlap extension PCR [16]. PTP-1B cloning primers (see above) were used as outer primers, and inner primers were 5′-GGACTCCAAAGGCAGGC-CATGTGGTAT-3′ (nt 727-701, the mutated nucleotide is underlined) and 5′-CACATGGCCTGCCTTTGGAGTC-CCTG-3′ (nt 705-730, the mutated nucleotide is underlined). The mutated PCR fragment was swapped onto pEYFP-PTP-1B, to generate pEYFP-PTP-1B(D181A).

2.1.8. pIR-B-RLuc and pIR-B-EYFP

The cDNA encoding human IR-B (nt 139-4287 of accession number M10051 with the following deviation: H171Y, T448I, and K492Q; contained in pIM-907, provided by A.S. Andersen, Novo Nordic). A PCR fragment covering the entire coding sequence was generated with the primers 5′-GTCAAAGCTTATGGGCACCGGGGGCCG-GCGGGG 3′ (nt 139-161, added *Hin*dIII site underlined) and 5′- TGACGGATCC**CG**GGAAGGATTGGACCGAG-GCAAGGT-3′ (nt 4284-4261, added *Bam*HI site is underlined, and nucleotides added for in-frame coding are shown in bold), using pIM-907 as the template. The *Hin*dIII–*Bam*HI fragment of the PCR product was excised and cloned into the *Hin*dIII/*Bam*HI sites of pRluc-N3 (Bio-Signal Packard), to generate pIR-B-RLuc, and into the HindIII/BamHI sites of pEYFP-N1, to generate pIR-B-EYFP.

2.1.9. pIR-A-RLuc and pIR-A-EYFP

The cDNA encoding human IR-A (nt 139-4287 of accession number M10051 with the following deviations: A deletion of nucleotides corresponding to exon 11, encoding R(744)KTSSGTGAEDP, and the variation H171Y, T448I, and K492Q; contained in pRiSl-288, provided by A.S. Andersen, Novo Nordic). Using pRiSl-288 as a template, a PCR fragment was generated with the primers used for pIR-B-RLuc and pIR-B-EYFP, which was cloned similarly into pRluc-N3 and pEYFP-N1, to generate pIR-A-RLuc and pIR-A-EYFP, respectively.

2.1.10. pCH1-3

For the generation of IGFR-IR-B chimeric receptors, the *Kpn*I–*Bam*HI fragment of pIGFR–RLuc, corresponding to IGFR residues 512-1367 (numbering of the IGFR protein sequence is according to accession number P08069) was swapped with chimeric sequences generated by overlap extension PCR using the outer primers 5′-CACCTCCACCACCACGTCGAAG-3′ (nt. 1530-1551) and 5′-TGACGGATCCCGGGAAGGATTGGACCGAG-GCAAGGT-3′ (cloning primer used for the generation of pIR-B-RLuc and pIR-B-EYFP. Three sets of inner primers (5′-CAACATCGCCAAGGGATCTCCGCTTCCT-TTCAGGTC-3′ and 5′-GAAAGGAAGCGGAGATCC-CTTGGCGATGTTGGGAATG-3′; 5′-GGGGCCGATG-ATAATATGGATGAAGTTTTCATATCC-3′ and 5′-GA-TATGAAAACTTCATCCATATTATCATCGGCCCCCT-CATC-3′; 5′-GAAGAACGACACCTCTGGGAAGCC-AGGCTCCATCTCCTCT-3′ and 5′-GATGGAGCCT-GGCTTCCCAGAGGTGTCGTTCTTCCAC-3′) were used for the generation of pCH1 (IGFR residues 1-740, IR-B residues 763-1382; numbering of the IR-B protein sequence is according to accession number P06213), pCH2 (IGFR residues 1-936, IR-B residues 957-1382), and pCH3 (IGFR residues 1-1274, IR-B residues 1299-1382). Similarly, chimeric PCR fragments (primers not shown) were swapped into pIGFR-EYFP, to generate pCH1-EYFP, pCH2-EYFP, and pCH3-EYFP, to be used for fluorescent images only.

An expression construct encoding the 291-residue human IGFBP-3 (accession number X64875) was prepared from human liver oligo-dT-primed cDNA. Specific primers containing a *Kpn*I site (5′-TGCAGGTACCATGCAG-CGGGCGCGACCCA-3′, nt 133-151) and an *Xho*I site (5′-GTACCTCGAGCTTGCTCTGCATGCTGTAGCA-3′, nt 1005-985) were used to generate a PCR product which was cloned into the *Kpn*I/*Xho*I sites of pcDNA3.1/Myc-His(+)A (Invitrogen), to generate pBP3mH.

All PCRs were carried out using *Pfu* DNA polymerase (Promega), and all constructs were verified by sequence analysis.

2.2. Cell culture, transfection

Human embryonic kidney 293T cells (293tsA1609neo) [17] were maintained in high glucose DMEM medium supplemented with 10% fetal bovine serum, 2 mM glutamine, nonessential amino acids, and gentamicin (Invitrogen). Cells were plated onto 6 cm tissue culture dishes, and were transfected 18 h later by calcium phosphate co-precipitation using 10 μg of plasmid DNA [18]. After 24 h, cells were replated onto 96-well plates (CulturPlate-96, White, Perkin-Elmer) (100,000 cells per well) and further incubated for 24 h before BRET analysis. For analysis by Western blotting, cells were replated after 24 h onto 24-well plates (500,000 cells per well), incubated for another 24 h, and then stimulated with 10 nM IGF-I or insulin for 10 min. Stimulated cells were lysed on ice with 50 mM Hepes pH 7.9, 150 mM sodium chloride, 10 mM EDTA, 1% Triton-X-100, 4 mM sodium orthovanadate, 10 mM sodium fluoride, supplemented with PMSF (1 mM), leupeptin (2 μg/mL), aprotinin (2 μg/mL), and iodacetamide (100 μM) for 10 min. The lysates were cleared by centrifugation for 20 min at 4 °C.

2.3. Western blotting

For immunovisualization of phosphorylated IGFR or IR, lysates were separated by reducing SDS-PAGE (10–20%

Tris–glycine gels), and blotted onto a polyvinylidene difluoride membrane (Millipore). The blots were blocked with 2% Tween 20, equilibrated in 50 mM Tris–HCl, 500 mM NaCl, 0.1% Tween 20, pH 9.0 (TST), and then incubated overnight at room temperature with primary antibody, a mouse monoclonal antibody against phosphotyrosine, PY99 (Santa Cruz) diluted 1:1000 in TST containing 1% fetal bovine serum. Blots were washed in TST, and further incubated for 1h at room temperature with peroxidase-conjugated secondary antibody (P0260, DAKO) diluted 1:2000 in TST, and then washed again with TST. The blots were developed using enhanced chemiluminescence (ECL, Amersham), and images were captured with a KODAK Image Station 1000. Equal amounts of recombinant receptors were loaded based on comparison of expression using a monoclonal against the IGFR β-subunit, CT-1 (Gropep).

2.4. Bioluminescence resonance energy transfer assay in living cells

Transfected cells were replated onto 96-well plates 24 h before analysis. The cells were washed gently in 20 mM sodium phosphate, pH 7.4, 130 mM sodium chloride, supplemented with calcium chloride (0.1 mg/L), magnesium chloride (0.1 mg/L), and glucose (1 g/L) (buffer A). Twenty min before measurement, 5 μl coelenterazine h (Sigma) was added from a working stock solution of 50 μM in buffer A, to a final concentration of 5 μM. The BRET reading was conducted on a POLARstar Optima (BMG Labtechnologies) instrument equipped with a 475/30 nm filter for measurement of the luciferase signal, and a 535/30 nm filter for measurement of the EYFP signal. The BRET signals were acquired for 1 min prior to stimulation with recombinant human IGF-I and IGF-II (both receptor grade, Diagnostic Systems Laboratories), or with recombinant human insulin (a gift from C. Kristensen, Novo Nordic). Volumes of 10 μL were automatically injected from stock solutions in buffer A to a final concentration of 3–50 nM. Following stimulation, readings were continued for 5 min. BRET ratios were calculated as [(emission at 535/30 nm)−(emission at 475/30 nm) × cf]/[emission at 475/30 nm], where cf = (emission at 535/30 nm)/(emission at 475/30 nm) for cells transfected with the appropriate RLuc construct alone (measured values of cf were approx. 0.3) [19]. BRET ratios were plotted as a function of time. For comparison of constructs and for measurement of dose dependence, the increase in BRET ratio 5 min after stimulation was calculated using the stable BRET ratio at 0–60 s as the zero level.

2.5. Miscellaneous procedures

IGFBP-3 and IGFBP-4 were expressed in 293T cells, and purified and quantified as previously described [20]. The purified IGFBPs (60 nM) were incubated (2 h) at 37 °C with IGF-I (30 nM) in the presence or absence of recombinant pregnancy-associated plasma protein-A (PAPP-A) (0.75 nM) [21]. In some experiments, inhibitory polyclonal antibodies against PAPP-A [22] were included at a concentration of 40 μg/mL. The reaction mixtures were added to cells and BRET signals were measured as described above.

2.6. Statistical analysis

Results are expressed as the mean ± S.D. Statistical comparisons were performed using ANOVA, followed by multiple comparisons. Results were considered statistically significant at $P < 0.05$.

3. Results

3.1. Bioluminescence resonance energy transfer (BRET) applied to the IGF-I receptor (IGFR)

Upon binding of insulin to IR, conformational changes in the intracellular portion of the receptor are believed to be associated with receptor autophosphorylation [7,23]. We sought to exploit this model in an assay based on bioluminescence resonance energy transfer (BRET) [24] for the real-time measurement of the stimulation of the closely related IGFR. The application of the BRET assay principle is based on the assumption that receptor stimulation causes the C-terminal domains of the two β-subunits to come into closer proximity.

Briefly, the BRET technology is useful for the measurement of protein–protein interactions in living cells [25]. To measure the interactions of two candidate proteins, one is fused to the 35 kDa *Renilla* luciferase (RLuc, the donor), and the other is fused to the 27 kDa enhanced yellow fluorescent protein (EYFP, the acceptor), a mutated variant of green fluorescent protein (GFP). The synthetic RLuc substrate, coelenterazine h, is able to permeate the cell membrane and is converted by RLuc under the emission of blue light of 480 nm. When EYFP is in close proximity (<100 Å), a nonradiative transfer of energy causes its excitation, and yellow/green light of 527 nm is emitted. The efficiency of this resonance energy transfer depends on the spectral overlap of the luciferase/fluorophore pair, and on the distance between them. To quantify the interaction between the two proteins, the BRET ratio is calculated as the amount of yellow/green light emitted by EYFP compared with the blue light emitted by RLuc, as detailed in Materials and methods. The BRET principle, as applied to IGFR, is illustrated in Fig. 1B.

In 293T cells co-transfected with pIGFR–RLuc (Table 1) and pEYFP, encoding soluble EYFP, a basal BRET signal was observed (Fig. 2A, left panel, crosses). In cells co-transfected with pIGFR–RLuc and pIGFR–EYFP, the BRET signal was increased, demonstrating a more

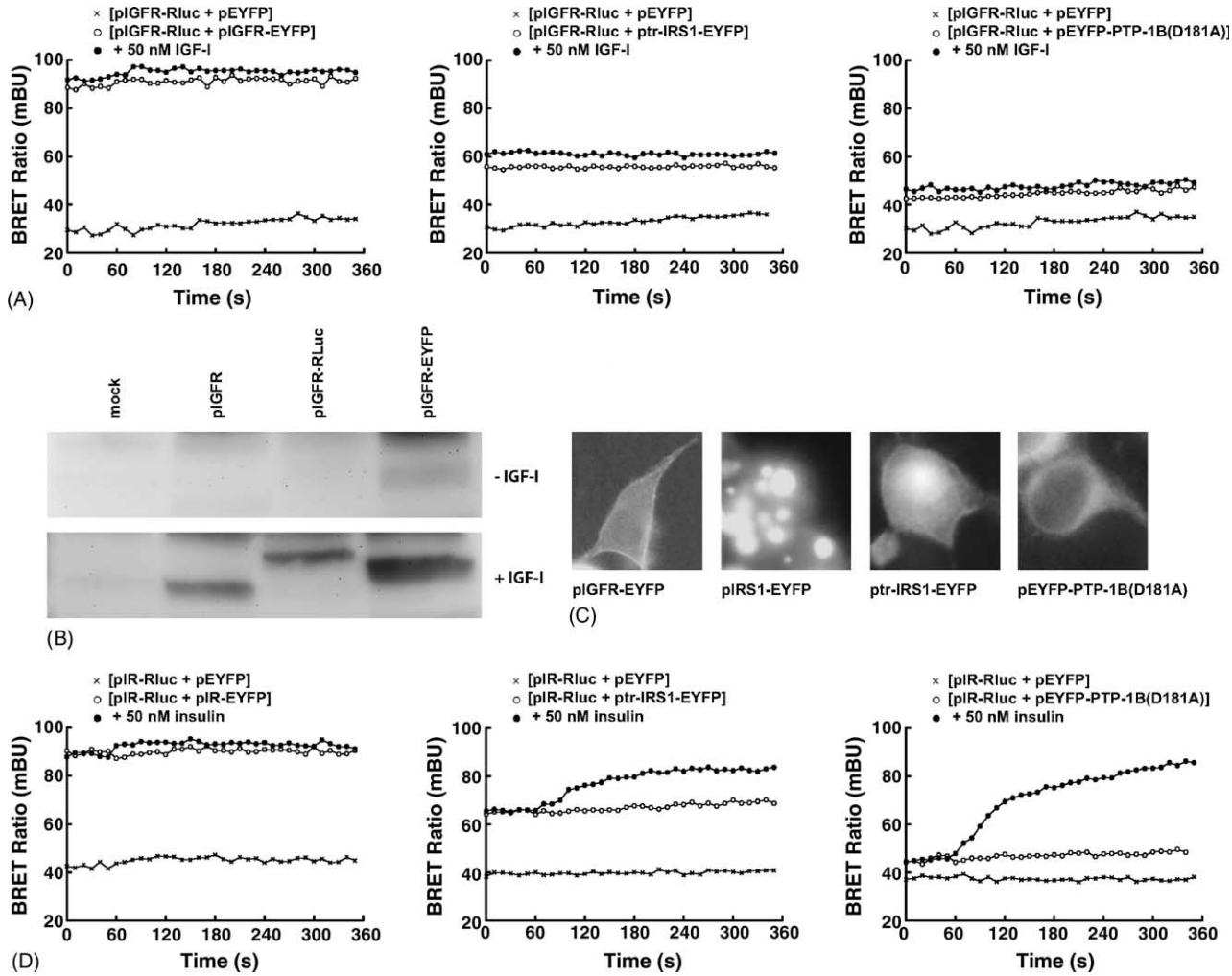

Fig. 2. Analysis of 293T cell transfected with RLuc- and EYFP-based fusion constructs. (A) Cells were co-transfected with pIGFR–RLuc and one of the following constructs as indicated (open circles): pIGFR–EYFP, ptr-IRS1–EYFP, and pEYFP-PTP-1B(D181A). The transfected cells were stimulated with 50 nM IGF-I (filled circles), at $t = 60$ s. Measured BRET ratios were plotted as a function of time (representative experiments are shown). In each series, analysis of cells co-transfected with pIGFR–RLuc and pEYFP (control plasmid pEYFP-N1 encoding soluble, EYFP), was included (crosses). (B) Western blotting of cell lysates using a monoclonal antibody specific for phosphotyrosine. Cells were transfected with empty vector (mock), pIGFR, pIGFR–RLuc, and pIGFR–EYFP, as indicated. Lysates from nonstimulated (upper panel) and stimulated cells (lower panel) are shown. The increased molecular weight of IGFR-RLuc (by 35 kDa) and IGFR-EYFP (by 27 kDa), is apparent. (C) Fluorescence microscopy showing the localization in transfected cells of IGFR–EYFP, IRS1–EYFP, tr-IRS1–EYFP, and EYFP-PTP-1B(D181A), as indicated. (D) Cells were co-transfected with pIR-B-RLuc and one of the following constructs as indicated (open circles): pIR-B-EYFP, ptr-IRS1–EYFP, and pEYFP-PTP-1B(D181A). The transfected cells were stimulated with 50 nM insulin (filled circles), at $t = 60$ s. Measured BRET ratios were plotted as a function of time (representative experiments are shown). In each series, analysis of cells co-transfected with pIR-B-RLuc and pEYFP (control plasmid pEYFP-N1 encoding soluble, nonfused EYFP), was included (crosses).

efficient donor-acceptor energy transfer when the luciferase/fluorophore pair is within the same molecule (Fig. 2A, left panel, open circles). However, the latter signal was not significantly increased upon stimulation with IGF-I (Fig. 2A, left panel, filled circles).

The fusion partners of IGFR do not appear to compromise receptor functionality, as the two fusion proteins both show the ability to autophosphorylate upon IGF-I stimulation (Fig. 2B), and IGFR–EYFP shows the expected localization in the cell membrane (Fig. 2C). However, the assumed conformational change affecting the distance between the luciferase and EYFP upon stimulation, may be too subtle, or the donor and/or the acceptor fluorophore may not be in a favorable orientation for increased BRET to occur.

3.2. Fusion of the acceptor fluorophore to downstream signaling molecules

As no increase in the BRET signal was obtained with both the donor and the acceptor fused to the subunits of IGFR, we analyzed the potential of IRS1 and the phosphatase PTP-1B, both known to interact directly with IGFR and IR, to function as alternative fusion partners for EYFP.

We first attempted to use a construct in which EYFP is fused C-terminally to wild-type IRS1 (pIRS1–EYFP).

However, based on fluorescence microscopy (Fig. 2C), it showed aberrant intracellular processing upon expression in 293T cells. A similar finding has previously been reported with wild-type IRS1 fusion protein [26]. However, in accordance with previous findings [26], EYFP fused to a truncated variant of IRS1 containing residues 1–262, encoded by ptr-IRS1–EYFP, appeared to distribute normally within transfected cells (Fig. 2C). We also prepared an expression construct, pEYFP-PTP-1B(D181A), in which EYFP is fused to a mutated variant of PTP-1B. This mutant, PTP-1B(D181A), is unable to dephosphorylate, but still binds to its substrates with high affinity [27]. Fluorescence microscopy showed the expected [28] localization within the transfected cells (Fig. 2C).

Both constructs, ptr-IRS1–EYFP and pEYFP-PTP-1B(D181A), were analyzed for their ability to function with pIGFR–RLuc in BRET assays. However, in both cases we did not see an increased BRET signal upon receptor stimulation (Fig. 2A, center and right panel).

3.3. BRET applied to the insulin receptor (IR-B)

Similar analyses were then carried out with the insulin receptor, following the preparation of two additional fusion constructs, pIR-B-RLuc and pIR-B-EYFP (Table 1), in which RLuc and EYFP, respectively, is fused to the C-terminal of IR-B. The ability of IR-B-RLuc to function in BRET analysis with IR-B-EYFP, tr-IRS1–EYFP, and EYFP-PTP-1B(D181A), respectively, was tested (Fig. 2D). With both the luciferase and the acceptor fluorophore fused to IR-B, we did not observe an increase in BRET signal upon insulin stimulation, similar to the results obtained with IGFR. Interestingly, however, with the acceptor fluorophore fused to the truncated variant of IRS1, tr-IRS1, a steady increase in the BRET signal was seen upon stimulation. Furthermore, using pIR-B-RLuc with pEYFP-PTP-1B(D181A), an even stronger BRET signal was observed. Assays for insulin based on intramolecular BRET of IR-B, and on intermolecular BRET between IR-B and PTP-1B have previously been reported [29,30]. Similarly, only a very week BRET signal was observed in the first assay setup, and a stronger signal in the latter.

Thus, assays based on the fusion of RLuc to the IR-B subunit, and EYFP to PTP-1B(D181A) or a truncated IRS1 (less sensitive) are functional (Fig. 2D). However, the same principles could not directly be applied for efficient measuring of IGFR stimulation (Fig. 2A).

3.4. A BRET assay for IGF based on IGFR/IR chimeras

In an attempt to obtain a BRET assay specific for the IGFs, but with the sensitivity of the IR-based assays, three plasmids encoding IGFR/IR chimeric receptors fused to RLuc were constructed (Fig. 3A). We also prepared an expression plasmid, IR-A-RLuc, encoding the IR-A variant

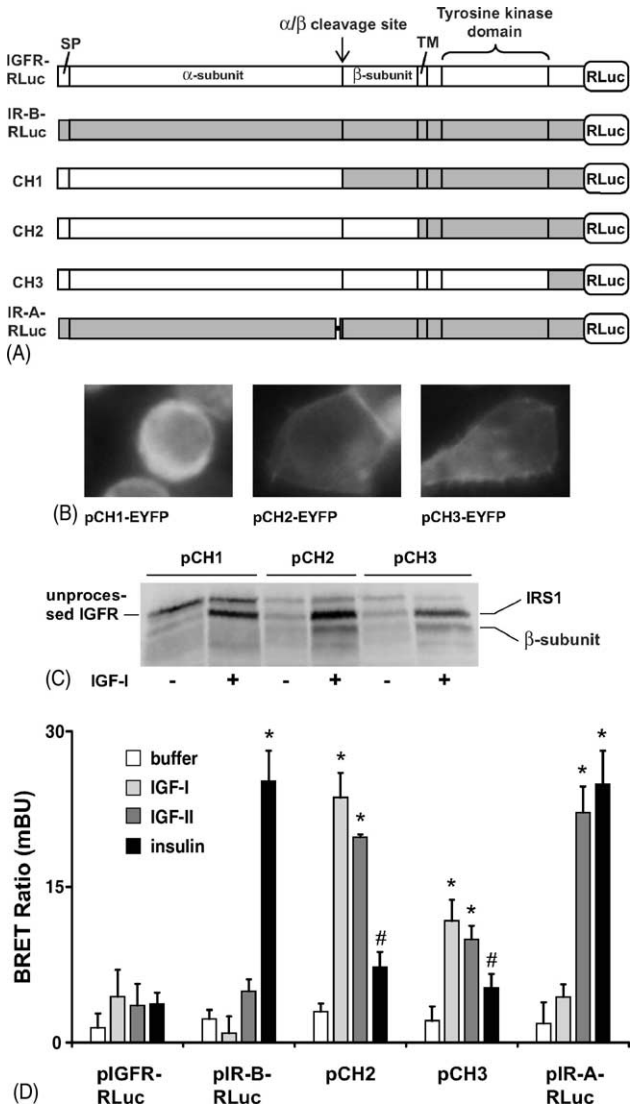

Fig. 3. Chimeras between IGFR and IR-B. (A) The fusion proteins encoded by pIGFR–RLuc and pIR-B-RLuc are depicted along with chimeras CH1, CH2, and CH3, in which a variable portion of IGFR sequence is replaced with sequence of IR. A fusion protein encoded by pIR-A-RLuc, in which the 12 residues of exon 11 of IR are lacking, is also shown. IGFR sequence is shown in white, and IR sequence is indicated by shading. (B) Fluorescence microscopy showing the localization in transfected cells of CH1-EYFP, CH2-EYFP, and CH3-EYFP, as indicated. (C) Western blotting using a monoclonal antibody specific for phosphotyrosine of 293T cells transfected with cDNA constructs as indicated. The positions of bands corresponding to unprocessed IGF proreceptor, the IGFR β-subunit, and IRS1 are indicated. (D) BRET ratios at $t = 300$ s obtained by co-transfection of 293T cells with the indicated constructs in combination with PTP-1B(D181A)-EYFP. The transfected cells were stimulated with buffer (white columns), 50 nM IGF-I (light grey columns), 50 nM IGF-II (dark grey columns), or 50 nM insulin (black columns). Values are averages of three experiments; standard deviations are indicated. (#) $P < 0.05$ vs. control; (*) $P < 0.01$ vs. control.

of the insulin receptor fused to RLuc (Fig. 3A). The IR-A variant of the insulin receptor differs structurally from IR-B by lacking 12 residues in the α-subunit (Fig. 3A), and functionally by showing increased binding of IGF-II compared to IR-B [11]. As judged by fluorescence microscopy, EYFP variants of chimeras CH2 and CH3 showed cellular

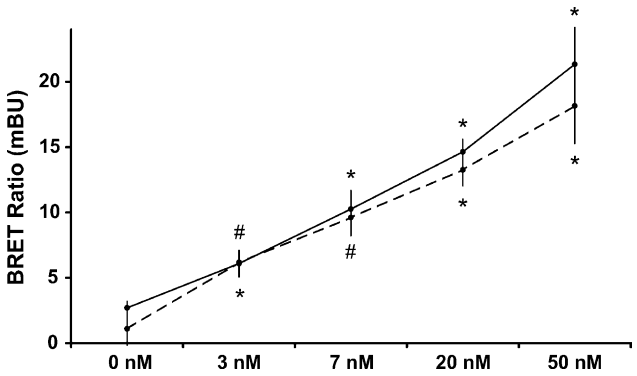

Fig. 4. Dose dependent BRET with IGFR-IR chimera CH2 and PTP-1B(D181A). Cells were co-transfected with pCH2 and pPTP-1B(D181A)-EYFP, and stimulated with increasing concentrations of IGF-I (solid line) or IGF-II (dashed line), as indicated. The measured BRET ratio at $t = 300$ s is plotted. Values are averages of three experiments; standard deviations are indicated. (#) $P < 0.05$ vs. previous concentration; (*) $P < 0.01$ vs. previous concentration. Indications are made above (IGF-I) or below (IGF-II) the lines.

localization similar to the wild-type receptors. CH1, in contrast, did not localize to the cell membrane (Fig. 3B). In accordance, Western blotting revealed anomalous processing of CH1, but not CH2 and CH3 (Fig. 3C).

Since PTP-1B(D181A) appeared to be the most efficient fusion partner for the acceptor fluorophore, cells were transfected with pPTP-1B(D181A)-EYFP combined with the chimeric RLuc constructs pCH2 and pCH3, or with pIR-A-RLuc, and BRET analysis was carried out with IGF-I, IGF-II, and insulin (Fig. 3D). Our results show that the assay based on CH2 is able to specifically detect both IGF-I and -II at a sensitivity comparable to the detection of insulin with the assay based on IR-B. The assay based on CH3 appeared to be less sensitive. Both insulin and IGF-II, but as expected not IGF-I, was sensitively detected with the assay based on IR-A.

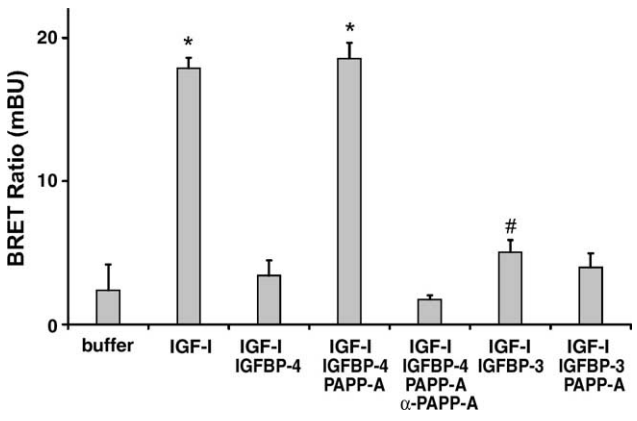

Fig. 5. Inhibition of IGFR stimulation by IGF binding proteins (IGFBPs). The effect of IGFBPs on receptor stimulation with IGF-I (30 nM) was analyzed. In some experiments, the proteinase PAPP-A which cleaves IGFBP-4, but not IGFBP-3, was included with or without the addition of inhibitory antibodies against PAPP-A. The combination of proteins in each experiment is indicated. Values are averages of three experiments; standard deviations are indicated. (#) $P < 0.05$ vs. control; (*) $P < 0.01$ vs. control.

In conclusion, with the assay based on pCH2 and pPTP-1B(D181A)-EYFP, specific IGF-I and -II activity can be measured. Analysis of ligand dose dependence shows that this assay is useful at ligand concentrations above 3 nM for both IGF-I and -II (Fig. 4), similar to previous results with IR-B [30].

3.5. Analysis of inhibitors of IGFR activity

Using the BRET assay, we analyzed the abilities of IGF binding protein (IGFBP)-3 and -4 to specifically inhibit IGF stimulation, and, in turn, the ability of the IGFBP-4 proteinase PAPP-A to circumvent this inhibition (Fig. 5). Complete inhibition of IGF-I activity was obtained with IGFBP-4. This inhibition was completely reversed by treatment with PAPP-A. In turn, polyclonal antibodies against PAPP-A, previously shown to inhibit its proteolytic activity [21], effectively abrogated the stimulatory effect of PAPP-A. In a similar manner, inhibition of IGF-I stimulation was obtained with IGFBP-3, but this effect was not reversed by PAPP-A (Fig. 5), in accordance with the substrate specificity of the enzyme.

4. Discussion

We have developed an assay based on bioluminescence resonance energy transfer that allows specific real-time measurement of IGF activity in living cells. The established system allows efficient screening for ligand- or receptor-directed molecules which inhibit IGF activity. In addition, we have demonstrated that a proteolytic enzyme, which cleaves and inactivates the inhibitory IGFBP-4, may function as a target to specifically inhibit IGF signaling by the inhibition of proteolytic activity.

Initial attempts to construct a BRET assay based on fusion of the luciferase (RLuc) to IGFR, and the acceptor fluorophore, EYFP to IGFR, or to the downstream signaling molecules, insulin receptor substrate-1 (IRS1) or protein tyrosine phosphatases-1B (PTP-1B), failed (Fig. 2A). However, similar experiments with IR, and IRS1 or PTP-1B, which we carried our in parallel, proved successful (Fig. 2D), in agreement with previous studies on IR and PTP-1B [30]. These results may be explained by subtle intracellular differences between IR and IGFR upon stimulation. Alternatively, as the strength of the BRET signal depends on favorable orientation between the donor and the acceptor, they may be a consequence of differences in the relative orientation of RLuc when fused to the two receptors. Interestingly, as the IR BRET assay appeared to function better with both IRS1 and PTP-1B, the RLuc may be in an unfavorable orientation when fused to IGFR.

We then successfully constructed assays based on chimeric IGFR/IR proteins, in which the ligand binding site was derived from IGFR (Fig. 3A). The most efficient assay was based on chimera CH2, in which the RLuc is fused to a

chimeric receptor with the entire intracellular portion derived from IR, and EYFP fused to PTP-1B. With this assay, we were able to measure IGF activity specifically with sensitivity similar to the corresponding assay for insulin, based on IR (Fig. 3D).

The ability to rapidly detect the stimulation of IGFR in living cells may facilitate the screening of compounds potentially agonizing or antagonizing the activities of IGF-I and/or -II. Such compounds may, for example, interfere directly with ligand-receptor interactions, allosterically influence receptor conformation, or interact with the tyrosine kinase domain to increase or decrease its activity [7]. These strategies to therapeutically control receptor activity are shared between IGFR and IR. However, the six IGF binding proteins (IGFBP-1–6) comprise an additional level of ligand-directed control of IGF activity in vivo [3]. Hence, the IGFBPs may function as alternative targets to specifically modulate IGF activity without affecting IR signaling. Furthermore, molecules which function to control the abilities of the IGFBPs to bind and inhibit the IGFs, may also prove to be valuable targets in the control of IGFR stimulation. The metzincin metalloproteinase pregnancy-associated plasma protein-A (PAPP-A) [20], which cleaves IGFBP-4 and -5 [31,32], is an obvious candidate target molecule, in particular because PAPP-A-null mice show a phenotype consistent with a complete lack of IGF-II signaling [33]. Specific inhibition of PAPP-A proteolytic activity may be relevant in pathological conditions such as atherosclerosis, where an increased level of PAPP-A is believed to be the underlying cause of increased IGF activity [34]. As example, we used IGFBP-3 and -4 to inhibit IGFR stimulation, and, in turn, PAPP-A to circumvent the inhibitory effect of IGFBP-4, but not IGFBP-3. These results emphasize the potential of specific inhibition of IGF signaling by targeting IGFBPs or molecules which control IGFBP activity, such as specific proteinases.

Compared to conventional assays for the measurement of IGFR stimulation, which involves lysis of cells prior to analysis, our assay measures receptor stimulation as it occurs in living cells. Such real-time measurement may be important in efforts to understand the kinetics of receptor stimulation, in particular differences in ligand binding mechanism between IGFR and IR. Additionally, it may prove valuable in the biochemical study of IGF release from IGFBP-IGF complexes in proximity to the cell surface [35].

Acknowledgements

We thank A.S. Andersen and C. Kristensen (Novo Nordic, Denmark) for providing insulin and cDNAs encoding IGFR, IR-B, and IR-A, and Diagnostic Systems Laboratories (TX, USA) for providing recombinant IGFs. The work presented here was supported by grants from the Novo Nordic Foundation, the Carlsberg Foundation, and the Danish Medical Research Council.

References

[1] Jones JI, Clemmons DR. Insulin-like growth factors and their binding proteins: biological actions. Endocrnol Rev 1995;16(1):3–34.
[2] Dupont J, LeRoith D. Insulin and insulin-like growth factor I receptors: similarities and differences in signal transduction. Horm Res 2001;55(Suppl. 2):22–6.
[3] Firth SM, Baxter RC. Cellular actions of the insulin-like growth factor binding proteins. Endocr Rev 2002;23(6):824–54.
[4] Jerome L, Shiry L, Leyland-Jones B. Deregulation of the IGF axis in cancer: epidemiological evidence and potential therapeutic interventions. Endocr Relat Cancer 2003;10(4):561–78.
[5] LeRoith D, Roberts Jr CT. The insulin-like growth factor system and cancer. Cancer Lett 2003;195(2):127–37.
[6] Pollak MN, Schernhammer ES, Hankinson SE. Insulin-like growth factors and neoplasia. Nat Rev Cancer 2004;4(7):505–18.
[7] De Meyts P, Whittaker J. Structural biology of insulin and IGF1 receptors: implications for drug design. Nat Rev Drug Discov 2002;1(10):769–83.
[8] Surmacz E. Growth factor receptors as therapeutic targets: strategies to inhibit the insulin-like growth factor I receptor. Oncogene 2003; 22(42):6589–97.
[9] Bahr C, Groner B. The insulin like growth factor-1 receptor (IGF-1R) as a drug target: novel approaches to cancer therapy. Growth Horm IGF Res 2004;14(4):287–95.
[10] Mitsiades CS, Mitsiades NS, McMullan CJ, Poulaki V, Shringarpure R, Akiyama M, et al. Inhibition of the insulin-like growth factor receptor-1 tyrosine kinase activity as a therapeutic strategy for multiple myeloma, other hematologic malignancies, and solid tumors. Cancer Cell 2004;5(3):221–30.
[11] Frasca F, Pandini G, Scalia P, Sciacca L, Mineo R, Costantino A, et al. Insulin receptor isoform A, a newly recognized, high-affinity insulin-like growth factor II receptor in fetal and cancer cells. Mol Cell Biol 1999;19(5):3278–88.
[12] Le Roith D, Bondy C, Yakar S, Liu JL, Butler A. The somatomedin hypothesis: 2001. Endocr Rev 2001;22(1):53–74.
[13] Kim JJ, Accili D. Signalling through IGF-I and insulin receptors: where is the specificity? Growth Horm IGF Res 2002;12(2):84–90.
[14] Buckley DA, Cheng A, Kiely PA, Tremblay ML, O'Connor R. Regulation of insulin-like growth factor type I (IGF-I) receptor kinase activity by protein tyrosine phosphatase 1B (PTP-1B) and enhanced IGF-I-mediated suppression of apoptosis and motility in PTP-1B-deficient fibroblasts. Mol Cell Biol 2002;22(7):1998–2010.
[15] Romsicki Y, Reece M, Gauthier JY, Asante-Appiah E, Kennedy BP. Protein tyrosine phosphatase-1B dephosphorylation of the insulin receptor occurs in a perinuclear endosome compartment in human embryonic kidney 293 cells. J Biol Chem 2004;279(13):12868–75.
[16] Ho SN, Hunt HD, Horton RM, Pullen JK, Pease LR. Site-directed mutagenesis by overlap extension using the polymerase chain reaction. Gene 1989;77(1):51–9.
[17] DuBridge RB, Tang P, Hsia HC, Leong PM, Miller JH, Calos MP. Analysis of mutation in human cells by using an Epstein-Barr virus shuttle system. Mol Cell Biol 1987;7(1):379–87.
[18] Pear WS, Nolan GP, Scott ML, Baltimore D. Production of high-titer helper-free retroviruses by transient transfection. Proc Natl Acad Sci USA 1993;90(18):8392–6.
[19] Angers S, Salahpour A, Joly E, Hilairet S, Chelsky D, Dennis M, et al. Detection of beta 2-adrenergic receptor dimerization in living cells using bioluminescence resonance energy transfer (BRET). Proc Natl Acad Sci USA 2000;97(7):3684–9.
[20] Boldt HB, Overgaard MT, Laursen LS, Weyer K, Sottrup-Jensen L, Oxvig C. Mutational analysis of the proteolytic domain of pregnancy-

associated plasma protein-A (PAPP-A): classification as a metzincin. Biochem J 2001;358(Part 2):359–67.

[21] Overgaard MT, Haaning J, Boldt HB, Olsen IM, Laursen LS, Christiansen M, et al. Expression of recombinant human pregnancy-associated plasma protein-A and identification of the proform of eosinophil major basic protein as its physiological inhibitor. J Biol Chem 2000;275(40):31128–33.

[22] Oxvig C, Sand O, Kristensen T, Kristensen L, Sottrup-Jensen L. Isolation and characterization of circulating complex between human pregnancy-associated plasma protein-A and proform of eosinophil major basic protein. Biochim Biophys Acta 1994;1201(3):415–23.

[23] Baron V, Kaliman P, Gautier N, Van Obberghen E. The insulin receptor activation process involves localized conformational changes. J Biol Chem 1992;267(32):23290–4.

[24] Xu Y, Piston DW, Johnson CH. A bioluminescence resonance energy transfer (BRET) system: application to interacting circadian clock proteins. Proc Natl Acad Sci USA 1999;96(1):151–6.

[25] Eidne KA, Kroeger KM, Hanyaloglu AC. Applications of novel resonance energy transfer techniques to study dynamic hormone receptor interactions in living cells. Trends Endocrinol Metab 2002;13(10):415–21.

[26] Jacobs AR, LeRoith D, Taylor SI. Insulin receptor substrate-1 pleckstrin homology and phosphotyrosine-binding domains are both involved in plasma membrane targeting. J Biol Chem 2001; 276(44):40795–802.

[27] Flint AJ, Tiganis T, Barford D, Tonks NK. Development of ''substrate-trapping'' mutants to identify physiological substrates of protein tyrosine phosphatases. Proc Natl Acad Sci USA 1997;94(5): 1680–5.

[28] Haj FG, Verveer PJ, Squire A, Neel BG, Bastiaens PI. Imaging sites of receptor dephosphorylation by PTP1B on the surface of the endoplasmic reticulum. Science 2002;295(5560):1708–11.

[29] Boute N, Pernet K, Issad T. Monitoring the activation state of the insulin receptor using bioluminescence resonance energy transfer. Mol Pharmacol 2001;60(4):640–5.

[30] Boute N, Boubekeur S, Lacasa D, Issad T. Dynamics of the interaction between the insulin receptor and protein tyrosine-phosphatase 1B in living cells. EMBO Rep 2003;4(3):313–9.

[31] Lawrence JB, Oxvig C, Overgaard MT, Sottrup-Jensen L, Gleich GJ, Hays LG, et al. The insulin-like growth factor (IGF)-dependent IGF binding protein-4 protease secreted by human fibroblasts is pregnancy-associated plasma protein-A. Proc Natl Acad Sci USA 1999;96(6): 3149–53.

[32] Laursen LS, Overgaard MT, Soe R, Boldt HB, Sottrup-Jensen L, Giudice LC, et al. Pregnancy-associated plasma protein-A (PAPP-A) cleaves insulin-like growth factor binding protein (IGFBP)-5 independent of IGF: implications for the mechanism of IGFBP-4 proteolysis by PAPP-A. FEBS Lett 2001;504(1–2):36–40.

[33] Conover CA, Bale LK, Overgaard MT, Johnstone EW, Laursen UH, Fuchtbauer EM, et al. Metalloproteinase pregnancy-associated plasma protein A is a critical growth regulatory factor during fetal development. Development 2004;131(5):1187–94.

[34] Bayes-Genis A, Conover CA, Overgaard MT, Bailey KR, Christiansen M, Holmes Jr DR, et al. Pregnancy-associated plasma protein A as a marker of acute coronary syndromes. N Engl J Med 2001;345(14): 1022–9.

[35] Laursen LS, Overgaard MT, Weyer K, Boldt HB, Ebbesen P, Christiansen M, et al. Cell surface targeting of pregnancy-associated plasma protein A proteolytic activity. J Biol Chem 2002;277(49):47225–34.